Synthesis and characterization of Ti_2AlC coatings by magnetron sputtering from three elemental targets and *ex-situ* annealing

C.Tang, M.Stueber, M.Klimenkov, U.Jaentsch, H.Leiste, M.Rinke, S.Ulrich, M.Steinbrück, H.J.Seifert

Institute for Applied Materials (IAM), Karlsruhe Institute of Technology (KIT), D-76021 Karlsruhe, Germany

Abstract:

MAX phase materials have demonstrated great potential applications both as bulk and coating due to their unique properties. Deposition of phase-pure polycrystalline MAX phase coatings often remains a challenge. In this study, Ti-C-Al elemental nanolayer stacks deposited by non-reactive magnetron sputtering followed by *ex-situ* annealing was adopted to prepare Ti_2AlC coatings on two different substrates, Si and SiO_2/Si. No Ti_2AlC phase was formed on Si substrate due to significant interdiffusion between the coating and the substrate during annealing. Phase-pure, i.e. single-phase Ti_2AlC coatings with 3 μm thickness on SiO_2/Si were obtained after 800°C annealing in argon for 10 min. The crystalline transition from the non-MAX competing phases to Ti_2AlC MAX phase was found to appear in the region of 600°C - 700°C. The microstructural evolution of the coatings during annealing from 600°C to 900°C was systematically investigated by X-Ray diffraction (XRD), Raman spectroscopy and transmission electron microscopy (TEM). The reaction path for the formation of Ti_2AlC is suggested as follows: first, aluminum reacted with titanium to form a Ti-Al intermetallic phase (i.e. Al_3Ti), and the diffusion between the residue titanium and carbon produced non-stoichiometric TiC_x; then, the reaction between the Al_3Ti intermetallic and TiC_x yielded the formation of Ti_2AlC MAX phase.

Key words: nanoscale multilayers; magnetron sputtering; annealing; Ti_2AlC MAX phase; microstructural evolution

1. Introduction

Materials denominated by the structure formula $M_{n+1}AX_n$, well-known as MAX, phases comprise an extended family of layered, hexagonal transition metal carbides and nitrides. Their distinctive structure can be described by a near-close-packed M layer (where M is an early transition metal), interleaved with layers consisting of pure A-group elements (i.e. mostly elements from groups 13 and 14), with the X atoms (X= C or N) filling the M_6X octahedral cages. The various n (typical 1-3) values represent different numbers of transition metal carbide and/or nitride layers separated by the A layers [1–3]. The majority of MAX phases discovered up to now are M_2AX with a smaller number of M_3AX_2, M_4AX_3 and solid solutions. Different kinds of chemical bonds, the strong covalent-ionic M-X bonds together with relatively weak metallic M-A bonds, co-exist within their layered structure, resulting in unique attributes combination of both ceramics and metals. Similar to their counterpart transition metal binary carbides and nitrides, MAX phase compounds possess low density, low thermal expansion coefficients, elastic stiffness and high melting points. Moreover, like metals, they exhibit easy machinability, high electrical and thermal conductivities, high ductility, thermal shock and damage tolerance, excellent high-temperature mechanical properties and sometimes fatigue and oxidation resistance [2,4]. Hence, MAX phase materials have shown promising application potential in the form of both bulk materials and thin films, for example as high temperature components [5], reinforced materials [6], nuclear claddings [7], and oxidant resistant [8] and tribologically protective [9] coatings. Their excellent properties also have stimulated a great deal of interest in figuring out the interplay of bonding, composition, and microstructure on properties by detailed experimental and theoretical investigations in recent decades.

In terms of synthesis of MAX phase compounds, original approaches focused on the preparation of relatively phase-pure bulk products. Several different process techniques have been developed; the most common and important method is hot isostatic pressing (HIP) by using corresponding stoichiometric elemental and/or binary ceramic powders. It has been demonstrated that relatively high temperature and pressure along with long synthesis time was required to ensure that the starting original materials completely transform to MAX phase. In most cases, a minor amount of impurities, usually counterpart binary carbides or nitrides, remain in the final products [10,11]. It has been recently confirmed that some MAX phases can be synthesized as thin films or coatings at relatively low temperature, several hundred degrees lower compared to the synthesis of bulk materials [3]. This provides an opportunity to utilize the properties of both MAX phases and substrate materials within convenient technological processes and at reduced costs. Various techniques have been developed for growth of MAX

phase thin films. A large part of pioneering work on synthesis of MAX phase thin films was performed using magnetron sputtering technology, either from elemental targets or from compound targets [12–20]. This process has the advantage of producing dense, single crystalline films or high purity polycrystalline films. The MAX phase can be produced *in-situ* during sputtering at high deposition (substrate) temperature or *ex-situ*, by deposition of nanoscale multilayers or amorphous films that are subject to subsequent annealing. In addition to magnetron sputtering, other PVD processes such as high power impulse magnetron sputtering (HIPIMS) [20], cathodic arc deposition [21], pulsed laser deposition [22] as well as chemical vapor deposition (CVD) [23], and spray techniques [24,25] were developed to synthesize MAX phase thin films.

In the Ti-Al-C ternary system, two MAX phases (Ti_2AlC and Ti_3AlC_2) exist, and both have been well-studied. One remarkable characteristic of these two MAX phases is their excellent high-temperature isothermal and cyclic oxidation resistance up to 1400°C both in air and in humid atmosphere [26,27]. Their excellent high-temperature oxidation resistance stems from the selective oxidation of aluminum and the small difference of the coefficients of thermal expansion (CTE) between Al_2O_3 and substrate contributing to the growth of a slow-growing, adherent, dense and protective α-Al_2O_3 layer during oxidation. Ti_2AlC shows slightly better high-temperature oxidation resistance due to its higher Al content compared to Ti_3AlC_2 [28]. Recent studies also demonstrated that Ti_2AlC can maintain phase stability and crystallinity during heavy ion irradiation and neutron irradiation even at exposure to high displacements per atom (dpa) [29,30]. These outstanding performances facilitate the investigation of using Ti_2AlC as protective coating on nuclear claddings in light water reactors (LWRs) to increase the safety margin during severe nuclear accidents [8]. Ti_2AlC and Ti_3AlC_2 thin films were first produced by Wilhelmsson et al. from co-deposition of three elemental targets on α-Al_2O_3 (0001) substrates [12]. Epitaxial MAX-phase thin films were grown at 900°C with high crystalline quality; the deposition at 700°C and 800°C resulted in the formation of cubic (Ti,Al)C and perovskite carbide Ti_3AlC phases, respectively[12,31,32]. Intensive studies were carried out since then to deposit Ti_2AlC MAX phase thin films on various substrates using different deposition processes; however the oxidation behavior and thermal and chemical stability of these films were investigated only partially. A TiC(111) seed layer was usually used to promote the epitaxial growth of MAX phase thin films in initial studies [31], while later investigations demonstrated that the MAX phase thin films can directly nucleate on the substrate [3,21]. Using also three element targets, Garkas et al. successfully prepared Ti_2AlC MAX phase coatings in an industrial-size coater at 800°C. They demonstrated that the coatings were unstable and completely decomposed after annealing at

1200°C for 1h in vacuum due to out-diffusion of Al followed by evaporation of Al [33]. Wang et al. synthesized Ti–Al–C thin films on polycrystalline Al_2O_3 specimens at 800°C which composed mainly of a Ti_2AlC phase with Ti_3AlC and TiC competitive second phases. During oxidation in air, the films were quickly oxidized at temperature higher than 700°C which was attributed to the microstructural characteristics of the films [34]. Reactive magnetron sputtering with a compound Ti50Al50 (at.%) target in Ar/CH_4 atmosphere was also used to produce Ti_2AlC protective coatings on stainless steel substrates, however, the coatings were not phase-pure and, moreover, contained through-cracks [35,36]. Attempts to deposit the Ti_2AlC MAX phase from one single compound target resulted in chemical composition of the produced films that deviated significantly from the composition of the target; both loss of Al [17] and Ti [37] were observed. This effect was enhanced with increasing deposition temperature which was attributed to re-evaporation of the adatoms during deposition [38]. A separate plasma source was needed to compensate the lost element when deposited from one compound target. Epitaxial single-phase growth of Ti_2AlC on α-Al_2O_3 (001) single crystal has been deposited by pulsed cathodic arc deposition using multi-cathodes at 900°C; substitutional O (residual gas in chamber) in some C lattice sites was observed for the Ti_2AlC films [21,39,40]. High velocity oxy-fuel spray [24,41,42] and cold spray processed [8,25] were also adopted to deposit thick Ti_2AlC coating as oxidation resistant coating from Ti_2AlC powders. However, the obtained coatings usually displayed a loose structure and contained second phases of Ti_3AlC_2, TiC and Ti-Al intermetallics. The coating performance may be reduced during service and further investigations to overcome these limitations are required. Based on the above findings, it can be concluded that several challenges, like deposition of phase-pure, especially polycrystalline pure MAX phase thin films, further reduction of the substrate temperature (for example when using magnetron sputtering processes) and the deposition of dense, thick coatings on technologically relevant substrates, still exist for the synthesis of Ti_2AlC MAX phase coatings. Recently, a rapid and easy method was successfully applied to the synthesis of polycrystalline Ti_3SiC_2 [43] and Cr_2AlC [13] thin films through magnetron sputtering from three individual elemental targets to obtain a periodical elemental multilayer stack and subsequent rapid thermal annealing. This method offers the possibility to control the stoichiometry of the films precisely and easily, and the results demonstrated that the crystallization temperature of the MAX phase was also lower than in previous investigations.

The motivation of this work is also about elaboration of the potential of synthesizing MAX phase coatings by post-annealing of nanoscale elemental multilayer films in the Ti-C-Al system. In this study we addressed the synthesis of relative thick (around 3 μm), polycrystalline Ti_2AlC MAX phase coatings through deposition of elemental multilayer stacks followed by *ex-situ* rapid

annealing in argon on two different substrates, Si and SiO_2/Si. The results will show that the crystalline transition from the non-MAX competing phases to Ti_2AlC MAX phase could be reduced to 600°C - 700°C, and phase-pure Ti_2AlC coatings were obtained after 800°C annealing for just 10 min. It will be discussed, that an appropriate selection of the substrate material, the nanoscale multilayer architecture and the annealing conditions is a pre-requisite for successful MAX phase formation from elemental multilayers in the Ti-C-Al system. The microstructural evolution during annealing from 600°C to 900°C was systematically investigated by X-ray diffraction (XRD), Raman spectroscopy and high resolution transmission electron microscopy (HRTEM). The mechanisms of reaction path and crystal growth are discussed on the basis of the above specified conditions.

2. Experimental

The Ti-C-Al coatings presented in this study were deposited by non-reactive magnetron sputtering from three 75 mm diameter cylindrical elemental targets of titanium, graphite and aluminum using laboratory PVD equipment (i.e. a Leybold Z 550 coater). A multilayer approach was adopted and the design of the layered stacks is shown in Fig.1. The thicknesses of each elemental layer were around 8 nm for titanium, 2 nm for carbon and 4 nm for aluminum, calculated according to the stoichiometric ratio of these three elements in Ti_2AlC and considering their theoretical densities. These low values for the thicknesses of each layer were selected in order to reduce the required diffusion distances. The sequence of the individual layers is titanium-carbon-aluminum. This periodical stack (with a thickness of 14 nm) has been repeated until a total film thickness of ~ 3 μm was obtained. Two types of substrates were used, Si(100) wafer and Si(100) wafer with an amorphous 1 μm thermally grown SiO_2 layer on the surface as they were substrates commonly used in PVD process and did not contain the elements of the Ti_2AlC phase. The substrates were cleaned in an ultrasonic bath in acetone for 10 min, and then fixed on a rotary sample holder at a distance of around 7 cm to the target. The vacuum chamber was evacuated to a base pressure of around $1x10^{-4}$ Pa. Prior to deposition, the substrates were plasma-etched at 500 W r.f. power in 0.5 Pa pure Ar atmosphere for 10 min. The etching rate was measured to be around 5 nm/min for pure Si substrate. For the deposition of the Ti-C-Al coatings, the working pressure of Ar was maintained at 0.5 Pa and the substrates were grounded. The magnetron power was set at 200 W for all three targets. These settings were used in separate experiments with individual titanium, carbon, and aluminum coatings dedicated to the determination of individual deposition rates. The measured deposition rates were 0.6 nm/s for Ti (RF power), 0.2 nm/s for C (DC power) and 1.1 nm/s for Al (RF power). During multilayer deposition, the PVD equipment run in a stop-and-go mode, i.e. the sample holder rotated from

one target position to another one and stayed for various holding times at each individual target position. A shutter was installed between the target and the substrate holder to only allow the deposition of one element at each position. Furthermore, the substrates were not heated.

After deposition, the samples were *ex-situ* annealed in pure Ar (99.9999%) atmosphere at atmospheric pressure using a commercial thermal balance (NETZSCH STA-449). The chamber was evacuated twice down to 1.0×10^{-2} Pa before filling with Ar. The annealing temperature was varied from 600°C to 900°C. The heating and the cooling rates were fixed at 10 K/min and the isothermal holding time was 10 min.

The overall chemical compositions of the coatings were determined by electron microprobe analysis (EPMA) using a Cameca microbeam system, and the elemental depth profiles, both the as-deposited and annealed coating, were measured by Auger electron spectroscopy (AES, PHI 680 Xi Auger Nanoprobe system). The microstructure of the coatings was characterized by X-ray diffraction (XRD, Seifert PAD II diffractometer), Raman spectroscopy (Renishaw Raman 1000 with 514.5 nm Ar ion laser excitation, using an incident power of 23 mW focused to a spot size of ~1 μm), atomic force microscopy (AFM, NanoScope® Dimension™ 3100 Controller in contact mode), scanning electron microscopy (SEM, Philips XL30S), and high resolution transmission electron microscopy (HRTEM, FEI Tecnai 20 FEG). For EPMA measurement, the measurements were repeated four times in different regions and the given data are average values of those. In case of XRD measurement, a classical θ-2θ diffraction experiment was applied using CuKα radiation (λ= 1.54Å) with a scan speed at 1 °/min and a step size of 0.002 °. The cross-sectional lamellas for HRTEM analyses were prepared by focused ion beam technique (FE-REM/FIB AurigaTM-Crossbeam System/Cobra FIB-Column, ZEISS Inc.). The TEM study was performed in bright-field mode with 200 kV acceleration voltages. The scanning transmission electron microscopy (STEM) using high angle annular dark field (HAADF) detector was applied for imaging and spatially resolved analytical characterization of thin layers. The elemental analysis was performed using an energy dispersive X-ray (EDX) detector (production of EDAX Inc.). A Berkovich micro-indenter (UMIS 2000) was used to measure the indentation hardness and reduced Young's modulus of the coatings. The indentation depth was adjusted significantly higher than the surface roughness but less than 1/10 of the total film thickness to avoid substrate effects. At least ten indentations were carried out on each sample and the values reported herein represent the average. A commercial Maxthal 211® bulk ceramic (nominally Ti_2AlC, Kanthal/Sweden) was used as reference for Raman spectroscopy analyses and hardness measurements.

3. Results

3.1. Coatings on pure Si substrate

The average elemental composition of the as-deposited coatings on pure Si substrate measured by EPMA is as follows: Ti: 50.5 at.%, C: 22.8 at.% and Al: 26.7 at.%. The results indicate that the composition of the films is overall very close to the ideal stoichiometry of Ti, C, Al (2:1:1) in bulk Ti_2AlC; the concentration of carbon is however slightly lower than the theoretical value. This can be explained by the density of the deposited carbon layer which usually is lower than the theoretical density of the graphite which was adopted here to calculate the single layer thickness [44]. The periodical nanoscale multilayer stacks of the as-deposited coatings are proved by both AES depth profiles and HRTEM images which will be shown in next section.

The cross-sectional SEM images of the as-deposited coatings and 800°C annealed coatings on Si are exhibited in Fig.2. It can be seen that the as-deposited coatings are dense, smooth, uniform and very fine-scale and do not show large growth defects. The growth of the coatings is columnar and the thickness of the coating is approximately 3.2 μm. As shown in Fig.2 (b), after annealing at 800°C for 10 min, the coatings show a completely different morphology, being more granular and rough, and exhibiting sub-micron scale pores and other defects. Moreover, the interface between the coating and the substrate becomes inconspicuous and obviously a reaction zone is formed. Fig.2(c) shows the EDS line-scan profile across this 800°C annealed coatings cross-section form the surface to the substrate. This result revealed that a significant amount of Si diffused into the coating and some Ti diffused into the substrate. The coating is obviously completely mixed up and shows a more or less homogeneous mixture of all elements, Ti, Al, C, and additionally Si. The distinctive multilayer structure is lost during this annealing. The XRD pattern of the coating on Si after annealing at 800°C is shown in Fig.3. A number of reflexes are visible, marked by black triangles in Figure 3. By detailed analysis of the diffraction patterns (and considering the results of the compositional analysis) all these reflexes could be attributed to various compounds, namely crystalline $Ti_7Al_5Si_{12}$ (PDF card No. 18-0071) and Al_4C_3 (PDF card No. 35-0799) phases. Thus, the annealed coatings are suggested to be composites of both these phases. A similar behavior has been observed for the synthesis of Ti_3SiC_2 MAX phase on Si [43]. The absence of a MAX phase and significant inter-diffusion between the coating and the substrate during annealing suggest that a diffusion barrier would be needed for synthesis of a MAX phase coating on Si or some metallic substrates [45].

3.2. Coatings on SiO_2/Si substrate

3.2.1. Composition

Fig.4 shows the AES depth profiles of four elements, Ti, Al, C, O in the as-deposited and 700°C and 800°C annealed samples on SiO_2/Si substrates. The as-deposited coating demonstrates clearly a periodical laminated structure with relatively sharp interface between the Ti, C, and Al elemental layers. The coating surface is contaminated by oxygen (due to exposure of the sample to the ambient) and is also rich in aluminum (as the top layer of the multilayer coating is aluminum). Further, the as-deposited coating is barely contaminated by oxygen or other elements (i.e. the oxygen content is about 1.5 at.%). The deposition at low temperature resulted in a low desorption rate of oxygen from residual gas that trapped the oxygen in the coating during growth [32].

The elemental layers completely diffuse and the distribution of each element become uniform during the annealing of the coatings at 700°C and 800°C for 10 min, as demonstrated in Fig.4 (b) and (c). There is no obvious difference between these two samples whereas the thickness of the surface oxide is significantly increased (by around 50 nm). This is a result of residual air trapping in the annealing oven or trace oxygen impurity in the argon gas. The oxidation of the surface zone could be avoided by direct annealing in the chamber after deposition without exposure to air; however, this cannot be fulfilled in our sputtering facility. The diffusion of Al toward the surface became more pronounced with the increasing annealing temperature. It can be seen that the Al content shifts to slightly lower concentration than that of C after annealing at 800°C compared to slightly higher concentration for the as-deposited and the 700°C annealed coatings. The concentrations of Ti, Al and C in the 800°C annealed coating was also determined by EPMA after removing the surface layer during the AES depth profile measurement. The normalized concentrations of Ti, C and Al were measured as 51.0 at.%, 26.2 at.% and 22.8 at.%, respectively. The values validated the observation that a minor amount of Al was lost due to diffusion toward the surface and oxidation.

3.2.2. Microstructure

The X-ray diffraction patterns of the as-deposited and annealed coatings on SiO_2/Si substrates are presented in Fig.5 for different annealing temperatures from 600°C to 900°C. Fig.5 (a) shows the results of the as-deposited coating. A relatively broad diffraction peak is observed at around 38°, close to the theoretical position of Ti (110) (PDF card No. 44-1294) and Al (111) (PDF card No. 04-0787) reflexes. The θ-2θ diffraction pattern demonstrates that the titanium and aluminum

layers are grown in nanocrystalline structure. The carbon layers, as expected, are grown in an amorphous network. After annealing at 600°C (c.f. in Fig.5 (b)), the XRD pattern shows a different character: nanocrystalline titanium and aluminum phases are not observed anymore, but the formation of the intermetallic compound Al_3Ti (PDF card No. 37-1146) and titanium carbide (PDF card No. 32-1383) are observed. The diffraction intensity originating from the titanium carbide reflex is however relatively weak and the signal is broad, suggesting that there is some carbon remaining in an amorphous state within the coating.

As the annealing temperature increases to 700°C, the diffraction intensity of Al_3Ti increases significantly probably because the diffusion of aluminum becomes extremely fast once the temperature reaches or exceeds the melting temperature of Al (around 660°C). Meanwhile, a Ti_2AlC MAX phase begins to crystallize and the Ti_2AlC (002) and (006) planes (PDF card No. 29-0095, $P6_3/mmc$ space group with a=0.304 nm and c=1.360 nm) [11] are clearly visible. The crystallization onset temperature of the Ti_2AlC phase synthesized by this method is in the range of 600°C – 700°C. The sample annealed at 800°C displays the formation of the pure Ti_2AlC MAX phase only. Thus, we claim this sample being single-phase Ti_2AlC. The formation of common competing binary and ternary phases in the Ti-Al-C system, like Ti-Al intermetallics, TiC, Ti_3AlC and Ti_3AlC_2 described in work published so far [12,17,35], during the deposition of Ti_2AlC MAX phase are not observed. The crystallinity of the Ti_2AlC MAX phase is enhanced at 800°C compared to that at 700°C, which means the crystallinity of the MAX phase is significantly dependent on thermally activated processes. The sharp and strong XRD signals at 13.01° and 39.74° generated by (002) and (006) planes, respectively, demonstrate a preferred orientation of (00l) basal planes. For the sample annealed at 900°C, the highest temperature in this study, the diffraction pattern is on a first view similar to that of the sample annealed at 800°C. However, some slight modification is visible: the diffraction intensity of the (002) plane decreases; the originally observed (006) lattice plane signal seems to overlap with a (103) lattice plane signal and a tiny shift of these to lower diffraction angles are noticed. This is probably due to the increasing diffusion rates at high temperature enabling the fast growth of Ti_2AlC grains along with loss of oriented growth, which will be discussed later in this paper.

Raman spectroscopy analyses were performed to further confirm the microstructure evolution and the formation of the Ti_2AlC MAX phase during annealing. Fig.6 shows the Raman spectra of the commercial Ti_2AlC bulk ceramic, as-deposited and annealed samples on SiO_2/Si substrates in the range of 160 cm^{-1} -2000 cm^{-1}. The spectrum of the commercial Ti_2AlC bulk ceramic is consistent with previous reports, and the Raman band of vibration modes E_{1g}&E_{2g} and A_{1g} are located at 258.1 cm^{-1} and 348.7 cm^{-1}, respectively, except for a little shift. For materials containing

amorphous carbon, the vibration modes of so-called D and G bands are usually located at around 1350 cm^{-1} and 1580 cm^{-1} [46]. Such spectral features are not observed at this region for bulk Ti_2AlC. However, the intensity of these two bands is significant in the as-deposited coatings, indicating the magnetron sputtered carbon layer is grown in amorphous state. With increasing annealing temperature, the D and G band intensities decrease dramatically and this amorphous carbon character disappears as shown by the Raman spectra of 800°C and 900°C annealed samples. The Raman active modes attributed to the Ti_2AlC MAX phase begin to become visible in the spectra after the coating is annealed at 700°C. For the 800°C and 900°C annealed coatings, the location of the observed signals fits quite well with the calculated values [47]. Table 1 summarizes the Raman active modes of Ti_2AlC MAX phase which were reported previously and observed in this study. These results further support the statement that Ti_2AlC starts to form at 700°C and a pure Ti_2AlC MAX phase is obtained at 800°C. A weaker band located at around 210 cm^{-1} for bulk Ti_2AlC ceramic and broader bands of lower intensity located in the range of 500 cm^{-1} -750 cm^{-1} except for the as-deposited coatings are also observed. These bands are supposed to be generated by the thin surface oxide and/or oxycarbide layer [48,49] as demonstrated by AES measurements and by non-stoichiometric TiC_x phase. Stoichiometric TiC has no Raman vibration modes but the introduction of disorder due to carbon vacancies make them Raman active [50]. The TiC_x phase exists as impurity in bulk Ti_2AlC and forms in the coatings at low annealing temperatures. The surface oxidation of the coatings also becomes more pronounced with increasing annealing temperature as shown in Fig.6.

Table 1 Raman active modes (cm^{-1}) of the commercial bulk Ti_2AlC and coatings obtained in this study

	E_{1g}&E_{2g}	**A_{1g}**	**Ref.**
Calculated	266	365	[47]
Experimental	260.9	370.3	[51]
Ti_2AlC bulk	264.6	358.7	This work
700°C annealed coating	261.5	342.2	This work
800°C annealed coating	266.8	362.9	This work
900°C annealed coating	269.0	359.7	This work

Fig.7 shows the AFM topography images of the as-deposited and 800°C annealed coatings on SiO_2/Si substrates. The surface is smooth with a roughness (Ra) value of only 5.0 nm for the as-deposited sample. The average roughness of the coating after 800°C annealing increases to 7.9 nm due to outward diffusion of Al during annealing. The surface and cross section of the as-received and 800°C annealing coatings on SiO_2/Si substrate were also investigated by SEM (see

Fig.8). The as-deposited coating is uniform and dense, free of holes, pores or other defects at this length scale. The coating thickness was around ~ 3.2 μm, in accordance with the coating on Si substrate. However, the coating annealed at 800°C shows a number of cracks; and cracks are also observed for coatings annealed at other temperatures, both on Si and SiO_2/Si substrates. The linear coefficients of thermal expansion (CTEs) of Si, amorphous SiO_2 and Ti_2AlC are 2.6 x 10^{-6} K^{-1}, 0.55 x 10^{-6} K^{-1} and ~8.7 x 10^{-6} K^{-1}, respectively [11,52,53]. The large CTE mismatch between the substrate and the coating contribute to induce cracking of the coating after annealing at high temperature. It is therefore suggested that a more suitable substrate or adhesive interlayer should be looked up for practical application of Ti_2AlC coatings synthesized by this method. The cross section SEM image in Fig.8 (d) shows that the interface between the coating and the amorphous SiO_2 diffusion barrier layer is clear, indicating that the interdiffusion between the substrate and MAX phase coating should be negligible.

In order to gather more insights into the microstructural evolution of the coatings during annealing, the as-deposited, as well as 700°C and 800°C annealed coatings were characterized by TEM. The cross sectional bright field TEM image of as-deposited Ti-C-Al coating on SiO_2/Si substrate is displayed in Fig.9. The layered stacks are confirmed by the different contrasts and the thickness of each layered stack is around 14 nm as planed and shown in the figure. The enlarged image below shows a detail of this nanoscale multilayer structure in higher magnification: it is clearly visible that the design follows the sequence of the titanium, –carbon, and –aluminum with titanium as the initial layer deposited on the substrate. The thickness of each layer is consistent with the estimated values according to deposition rates and the interface between each layer is clearly visible. The carbon layer is amorphous and the other two metal layers are nanocrystalline. Fig.10 shows a typical HRTEM image of the coating microstructure after annealing at 700°C. In full agreement with the previously described XRD results, it is confirmed that different nanocrystalline phases are observed: TiC, Al_3Ti, and the MAX phase Ti_2AlC. The crystallization of the Ti_2AlC MAX phase is shown without doubt, despite its volume content is low. The principal phase in the coating annealed at 700°C is identified as Al_3Ti. A relatively small amount of TiC_x phase can be seen (we denote the phase TiC_x as its stoichiometry may deviate from the perfect stoichiometry).

Fig.11 illustrates the plan-view bright field TEM images and the corresponding FFT image of the coating annealed at 800°C. As shown in Fig.11 (a), the coating fully crystallized with grain sizes around 20 nm. The strong overlapping of these nano-sized grains in the image plane prevents their clear TEM imaging. The typical nanolaminated microstructure of the MAX phase is shown. The coating shows a preference orientation of (00l) basal plane as demonstrated in the

inserted FFT image. The measured d-spacing in Fig.11 (b) is quite consistent with the theoretical value of the (001) plane of the Ti_2AlC MAX phase. No secondary glass phases in the grain boundaries and no evident impurity phases are detected. Fig.11 (c) shows the fast-Fourier transformed image of area B, which is indexed as [1-210].

The interface between the amorphous SiO_2 layer and the coatings was also investigated by TEM. The plan-view bright field TEM image of this interface is shown in Fig.12 (a) for a coating annealed at 800°C. A thin interdiffusion layer, around 20 nm thick, is clearly visible. Fig.12 (b) shows the HRTEM image of the interface. It can be seen that the SiO_2 substrate scale is amorphous, whereas, the diffusion layer displays a crystalline structure. The interface between the coating and the diffusion layer is uniform, however, the interface between the diffusion layer and the amorphous SiO_2 substrate scale becomes rough, demonstrating mainly the coating element diffuses into the substrate. No intergrown phases were observed between the coating and the diffusion layer. The EDS line-scanning results along the line in Fig.12 (a) from A to B is given in Fig.12 (c).The profiles reveal that the major diffusion species is Al, and a small amount of Ti in the coating also diffuses into the substrate. This suggests that the Ti_2AlC MAX phase directly nucleate and grow on the substrate with a (00l) preferred orientation, following by fast diffusion out of Al during annealing.

3.2.3. Mechanical characterization

The hardness and reduced Young's modulus with the standard deviation of the bulk Ti_2AlC ceramic and the Ti_2AlC coatings measured by microindentation are displayed in Fig.13. The measured indentation hardness and reduced Young's modulus of bulk Ti_2AlC are 4.3 ± 1.1 GPa and 158.7 ± 28.3 GPa, respectively. These values are in accordance with previous literature data [11]. The low hardness of MAX phase ceramic is attributed to the relatively weak bonds between TiC slabs and Al layers causing easy basal plane slip upon deformation [4]. The relative large fluctuation can be explained by the phase purity of the ceramic, which has been confirmed to contain a certain amount of TiC and Ti_3AlC_2 impurities [41]. For the as-deposited coating, the indentation hardness and reduced Young's modulus are around 7.6 GPa and 124.1 GPa. The measured values of hardness for the annealed coatings from 700°C to 900°C are in the range of 13 GPa -18 GPa, approximate 3-5 times higher than the value of bulk Ti_2AlC, and are similar to MAX phase coatings deposited by magnetron sputtering [12,16,29]. The indentation hardness first increases with increasing of annealing temperature (up to 800°C), and then slightly decreases upon the annealing temperature reaching 900°C. The highest level of indentation hardness is

observed at 800°C with a value of 17.2 GPa. The reduced Young's modulus gradually increased in the whole range of annealing temperature, reaching 270.3 GPa at 900°C.

Considering the hardness is the response of a material's ability to resist deformation upon loading, it is significantly affected by the composition and the microstructure of the materials. Moreover, compared to polycrystalline bulk materials, thin film often shows anisotropic hardness due to somewhat preferred orientation. Based on the microstructure evolution of the coatings annealed at different temperature, it is possible to understand the trend of change of the indentation hardness and reduced Young's modulus. Due to the formation of the nanocrystalline and enhanced crystallinity of Ti_2AlC MAX phase upon annealing from 700°C to 800°C, the indentation hardness and reduced Young's modulus gradually increase. The measured values scatter considerably at 700°C due to the formation of metallic and ceramic mixture phases. The decreasing hardness of the coatings after annealing at 900°C can be explained by the growth of the Ti_2AlC grains, elimination of preferred orientation, and probably removal of some growth defects [16].

4. Discussion

The crystal structure of MAX phases can be described as nearly-close-packed M layers with the X atoms filling the octahedral sites which are periodically interleaved by group-A elemental layers. The large unit cells determine their long c-axes characteristic, being around 13 Å for M_2AX phases [4]. Hence, it has been well acknowledged that the sputter-growth of MAX phase films requires significant thermal activation to enable sufficient mobility and energy for the desired atomic arrangement [3,11,16,32,54]. Lower deposition temperatures usually result in the formation of corresponding carbides and/or intermetallic phases. When it comes to Ti_2AlC physical vapor deposition, the most common temperature reported previously for the formation of MAX phase was equal to or higher than 800°C [12,32,33,35,40], except that one approach succeeded at 700°C [17], by depositing from one target or simultaneously from multiple targets. This work demonstrates that the crystalline transition from the non-MAX competing phases to Ti_2AlC MAX phase formation can be reduced to temperatures in the region of 600 °C - 700°C through the adoption of elemental nano-layered coatings and subsequent annealing. It is suggested that this decrease of the MAX phase formation temperature is attributed to nanoscale effects, such as higher surface activity in nanoscale and nanocrystalline materials. It is further suggested that such "topologically activated" materials exhibit other diffusion behavior (i.e. shorter diffusion length) than related bulk materials. The relatively lower-temperature synthesis

realized in this work appeals for synthesis of Ti_2AlC MAX phase onto temperature-sensitive substrate materials.

In this study, a reaction path for the formation of Ti_2AlC MAX phase coating has been demonstrated similar to the synthesis of bulk Ti_2AlC ceramic using a stoichiometric mixture of Ti, Al and graphite powder [55–57]. As shown by the XRD and TEM observations, first, Al reacts with Ti to form a Ti-Al intermetallic phase, Al_3Ti, and the diffusion and reaction between the residual Ti and C produce non-stoichiometric TiC_x. The former reaction is supposed to be enhanced once the annealing temperature approaches the melting point of Al as the signal intensity in X-ray diffraction analyses of Al_3Ti significantly increases from 600°C to 700°C. In a second step (at 700°C), the reaction between intermetallic Al_3Ti and TiC_x results in the formation of the Ti_2AlC MAX phase. One slight difference compared to the synthesis of bulk Ti_2AlC is that several Ti-Al intermetallic compounds are observed, and then transform to TiAl equilibrium phase for bulk materials [57]. In this study, only one Ti-Al intermetallic phase, Al_3Ti, is found, and no transformation is observed. One explanation can be that the synthesis of bulk materials is close to the thermodynamic equilibrium state; however, the crystallization of the MAX phase coating occurs at relatively low temperature compare to the bulk in non-equilibrium condition [3]. The formation mechanism of the Ti_2AlC MAX phase coating in this study can be described by the following potential reactions:

$$3Al + Ti \rightarrow Al_3Ti \qquad (1)$$

$$Ti + xC \rightarrow TiC_x \ (0 < x < 1) \qquad (2)$$

$$Al_3Ti + TiC_x \rightarrow Ti_2AlC \qquad (3)$$

The crystallization onset temperature for the formation of the Ti_2AlC phase in this study is by about 500 K lower than that of bulk Ti_2AlC, being around 700°C in this study and 1200°C for bulk materials, respectively [11].

It is necessary to note that the reaction path for the formation of the Ti_2AlC MAX phase by annealing of elemental layers in our study shows distinct deviation from previous investigations on deposition synthesis of Ti_2AlC through *in-situ* heating of the substrates. Deposition with *in-situ* heating at elevated temperature can successively lead to the formation of cubic (Ti,Al)C, then perovskite carbide Ti_3AlC, and finally the Ti_2AlC MAX phase with increasing substrate temperature [12,32,33]. Maintaining the substrate temperature at a certain level during deposition allows for a sufficient diffusion of each element to form the corresponding stable phase. However, in this study the annealing period is considerably shorter and the specific arrangement

of the elemental multilayer coating can support the thermodynamically preferred reaction of Al with Ti to form the Ti-Al intermetallic phase. Adjusting the multilayer nanoscale architecture according to the desired stoichiometry of the final MAX phase and taking into account mutual diffusion of the individual elements (as well as the heat of formation of the various phases and compounds) could offer a new tool for tailor-made synthesis of MAX phase materials. However it has to be recognized that such processing would require detailed thermodynamic and kinetic calculations and simulations.

One challenging issue during the synthesis of MAX phase coatings is to obtain the high purity MAX phases. A relatively narrow window of the composition close to the stoichiometry is a prerequisite for the synthesis of a homogenous MAX phase, where a small deviation from the stoichiometry results in impurity phases or even unwanted third phases. A small amount of impurity phases, often binary carbides, has been proved to reduce the performance of the coatings, such as oxidation resistance [34] and electrical conductivity [12]. Sputtering from one compound target usually results in off-stoichiometric composition of the films, often deviating strongly from the target. The use of three elemental targets has advantages of providing more flexible and powerful control of each elemental flux. However, previous studies which aimed to produce Ti_2AlC film by co-deposition from three targets could not completely avoid the growth of impurity phases. Diffraction patterns of TiC and Ti_3AlC phase, apart from Ti_2AlC, were sometimes clearly observed from the XRD results [12,34,35]. This can be explained by gas-phase scattering effects and/or interaction of each elemental atom during the gas-transport process [3]. However, formation of Ti_3AlC, one of the three stable ternary carbides in the Ti-C-Al system, has been proven to be deleterious to obtain high purity Ti_2AlC MAX phase due to the relatively high temperature needed for producing Ti_2AlC from Ti_3AlC and other compounds [55,58]. The Ti-C-Al elemental nano-multilayer stacks deposited from three individual targets at a time in this study can avoid this problem by precisely controlling the composition of the coating. Phase pure MAX phase can be obtained by subsequent annealing of this elemental layer system.

Previous studies on magnetron sputtering of MAX phase coatings mainly focused on epitaxial growth of MAX phase thin films on single crystal substrates, like MgO(111) [31,59–61] and Al_2O_3(0001) [12,32,39]. Basal-plane-oriented growth of MAX phase films are typically obtained due to the small mismatch of lattice parameters between the film and the substrate. Growth of MAX phases on amorphous or polycrystalline substrates usually leads to coatings with non-oriented polycrystalline microstructure [35,37]. It is worth to mention that the Ti_2AlC MAX phase coating after annealing at 800°C in this study shows a (000l) basal plane preferred-orientation. This phenomenon is clearly seen at the interface between the SiO_2/Si substrate and

the Ti_2AlC coating as demonstrated by TEM in Fig.12. Deposition of Ti_2AlC coating from Ti_2AlC powder on stainless steel substrates by high velocity oxy-fuel spraying had shown the same preferred orientation [41]. It is proposed that at the initial stage of crystallization the nuclei of many orientations form, however, the morphology is determined by the relative growth rates of all possible orientations [62]. The face with the lowest growth rate will determine the orientation of the grains. It has been demonstrated that the growth rate along *c* axes is much lower than that of *a* axes for the MAX phases [63]. Another possible explanation is that the (000l) surface may have the lowest surface energy, which appeals to terminate on the grain surface [64]. Both effects result in the growth of Ti_2AlC grains with *c* axis normal preferred orientation, and similar behavior has been observed sometimes in the preparation of bulk MAX phase ceramic [3,4]. The Ti_2AlC coating in this study after annealing at 900°C tends to lose the preferred orientation as seen in the XRD patterns, and this can be attributed to coalescence growth of Ti_2AlC MAX phase nanocrystals which are thermally activated by the high temperature. It can be predicted that the microstructure of the Ti_2AlC MAX phase coatings deposited by this method is significantly influenced by the annealing temperature and the annealing time.

5. Conclusions

This study attempted to synthesize phase-pure polycrystalline Ti_2AlC MAX phase coatings on two different substrates, Si wafer and Si wafer with an amorphous 1 μm thermally grown SiO_2 layer, by using Ti-C-Al elemental nano-multilayer stacks deposited by non-reactive magnetron sputtering from three targets accompanied by subsequent *ex-situ* annealing in argon. The results demonstrated that the titanium and aluminum layers were nanocrystalline and the carbon layer was amorphous in the as-deposited coatings. There was no MAX phase formation on Si substrates after annealing due to significant interdiffusion between the coating and the substrate, indicating a diffusion barrier was needed for synthesis of MAX phase coatings on Si (or some metallic substrates). Annealing of the coating on SiO_2/Si substrate at 600°C resulted in the formation of a mixed intermetallic Al_3Ti and titanium carbide. The crystalline transition from the competing non-MAX phases to Ti_2AlC MAX phase was located in the region of 600°C - 700°C. Phase-pure Ti_2AlC coating was obtained after 800°C annealing for 10 min with an average grain size around 20 nm. The 800°C annealed coating also displayed a preferred orientation of (000l) basal plane perhaps because of lower growth rate along *c* axes and the lowest surface energy of the (000l) surface in MAX phases. The coating after annealing at 900°C lost the preferred orientation attributed to coalescence growth of Ti_2AlC MAX phase nanocrystals which are thermally activated by the high temperature. The hardness of the coatings, a reflection of the

microstructural evolution, firstly increased with increasing of annealing temperature up to 800°C, reaching 17.72 GPa, and then slightly decreased upon the annealing temperature reaching 900°C.

Deposition of elemental nano-multilayer stacks from individual elemental targets in this study has shown the advantages of providing more flexible and powerful controlling of each elemental flux. The special arrangement of the elemental layer system, just 10 nm for the thickest layer (Ti), guaranteed a short diffusion length and higher surface activity due to nanoscale effects, leading to successful synthesis of pure Ti_2AlC coating at relative low temperature. Adjusting the multilayer nanoscale architecture according to the desired stoichiometry of the final MAX phase and taking into account mutual diffusion of the individual elements could offer a new tool for tailor-made synthesis of phase-pure MAX phase materials. The phase-pure coating will certainly be beneficial for practical application like as oxidation- and corrosion-resistant coating.

Acknowledgment

This work was supported by the Helmholtz (HGF) program NUSAFE and STN at the Karlsruhe Institute of Technology. It was further partially carried out with support of the Karlsruhe Nano Micro Facility (KNMF, www.knmf.kit.edu), a Helmholtz research infrastructure at the Karlsruhe Institute of Technology (KIT, www.kit.edu). C. Tang thanks for the PhD fellowship funded by the China Scholarship Council (CSC). The authors also thank Mr. T. Weingaertner, Dr. J.Ye, Mr. M. Strafela for helpful discussions. C. Tang especially appreciates the support, advice and technical assistance of Mr. S. Zils in thin film deposition.

Reference

[1] M.W. Barsoum, The $M_{N+1}AX_N$ phases: a new class of solids; thermodynamically stable nanolaminates, Prog. Solid State Chem. 28 (2000) 201–281. doi:10.1016/S0079-6786(00)00006-6.

[2] Z.M. Sun, Progress in research and development on MAX phases: a family of layered ternary compounds, Int. Mater. Rev. 56 (2011) 143–166. doi:10.1179/1743280410Y.0000000001.

[3] P. Eklund, M. Beckers, U. Jansson, H. Högberg, L. Hultman, The $M_{n+1}AX_n$ phases: Materials science and thin-film processing, Thin Solid Films. 518 (2010) 1851–1878. doi:10.1016/j.tsf.2009.07.184.

[4] M.W. Barsoum, MAX phases: properties of machinable ternary carbides and nitrides, John Wiley & Sons, 2013.

[5] M. Sundberg, G. Malmqvist, A. Magnusson, T. El-Raghy, Alumina forming high temperature silicides and carbides, Ceram. Int. 30 (2004) 1899–1904. doi:10.1016/j.ceramint.2003.12.046.

[6] S. Amini, M.W. Barsoum, On the effect of texture on the mechanical and damping properties of nanocrystalline Mg-matrix composites reinforced with MAX phases, Mater. Sci. Eng. A. 527 (2010) 3707–3718. doi:10.1016/j.msea.2010.01.073.

[7] E.N. Hoffman, D.W. Vinson, R.L. Sindelar, D.J. Tallman, G. Kohse, M.W. Barsoum, MAX phase carbides and nitrides: Properties for future nuclear power plant in-core applications and neutron transmutation analysis, Nucl. Eng. Des. 244 (2012) 17–24. doi:10.1016/j.nucengdes.2011.12.009.

[8] B.R. Maier, B.L. Garcia-Diaz, B. Hauch, L.C. Olson, R.L. Sindelar, K. Sridharan, Cold spray deposition of Ti_2AlC coatings for improved nuclear fuel cladding, J. Nucl. Mater. 466 (2015) 712–717. doi:10.1016/j.jnucmat.2015.06.028.

[9] M. Hopfeld, R. Grieseler, A. Vogel, H. Romanus, P. Schaaf, Tribological behavior of selected Mn+1AXn phase thin films on silicon substrates, Surf. Coatings Technol. 257 (2014) 286–294. doi:10.1016/j.surfcoat.2014.08.034.

[10] M.W. Barsoum, T. El-Raghy, Synthesis and characterization of a remarkable ceramic: Ti_3SiC_2, J. Am. Ceram. Soc. 79 (1996) 1953–1956. doi:10.1111/j.1151-2916.1996.tb08018.x.

[11] X.H. Wang, Y.C. Zhou, Layered Machinable and Electrically Conductive Ti_2AlC and Ti_3AlC_2 Ceramics: A Review, J. Mater. Sci. Technol. 26 (2010) 385–416. doi:10.1016/S1005-0302(10)60064-3.

[12] O. Wilhelmsson, J.P. Palmquist, T. Nyberg, U. Jansson, Deposition of Ti_2AlC and Ti_3AlC_2 epitaxial films by magnetron sputtering, Appl. Phys. Lett. 85 (2004) 1066–1068. doi:10.1063/1.1780597.

[13] R. Grieseler, B. Hähnlein, M. Stubenrauch, T. Kups, M. Wilke, M. Hopfeld, et al., Nanostructured plasma etched, magnetron sputtered nanolaminar Cr_2AlC MAX phase thin films, Appl. Surf. Sci. 292 (2014) 997–1001. doi:10.1016/j.apsusc.2013.12.099.

[14] M. Beckers, N. Schell, R.M.S. Martins, A. Mücklich, W. Möller, Phase stability of epitaxially grown Ti_2AlN thin films, Appl. Phys. Lett. 89 (2006) 74101. doi:10.1063/1.2335681.

[15] J. Emmerlich, D. Music, P. Eklund, O. Wilhelmsson, U. Jansson, J.M. Schneider, et al., Thermal stability of Ti_3SiC_2 thin films, Acta Mater. 55 (2007) 1479–1488. doi:10.1016/j.actamat.2006.10.010.

[16] Z. Wang, X. Li, J. Zhou, P. Liu, Q. Huang, P. Ke, et al., Microstructure evolution of V–Al–C coatings synthesized from a V_2AlC compound target after vacuum annealing treatment, J. Alloys Compd. 661 (2016) 476–482. doi:10.1016/j.jallcom.2015.11.170.

[17] J. Frodelius, P. Eklund, M. Beckers, P.O.Å. Persson, H. Högberg, L. Hultman, Sputter deposition from a Ti2AlC target: Process characterization and conditions for growth of Ti_2AlC, Thin Solid Films. 518 (2010) 1621–1626. doi:10.1016/j.tsf.2009.11.059.

[18] A. Abdulkadhim, T. Takahashi, D. Music, F. Munnik, J.M. Schneider, MAX phase formation by intercalation upon annealing of TiC_x/Al ($0.4<x<1$) bilayer thin films, Acta Mater. 59 (2011) 6168–6175. doi:10.1016/j.actamat.2011.06.029.

[19] H. Högberg, J. Emmerlich, P. Eklund, O. Wilhelmsson, J.P. Palmquist, U. Jansson, et al., Growth and Property Characterization of Epitaxial MAX-Phase Thin Films from the Tin+1(Si, Ge, Sn)Cn Systems, Adv. Sci. Technol. 45 (2006) 2648–2655. doi:10.4028/www.scientific.net/AST.45.2648.

[20] O. Berger, C. Leyens, S. Heinze, R. Boucher, M. Ruhnow, Characterization of Cr–Al–C and Cr–Al–C–Y films synthesized by High Power Impulse Magnetron Sputtering at a low deposition temperature, Thin Solid Films. 580 (2015) 6–11. doi:10.1016/j.tsf.2015.03.008.

[21] M.C. Guenette, M.D. Tucker, M. Ionescu, M.M.M. Bilek, D.R. McKenzie, Cathodic arc co-deposition of highly oriented hexagonal Ti and Ti_2AlC MAX phase thin films, Thin Solid Films. 519 (2010) 766–769.

doi:10.1016/j.tsf.2010.09.007.

[22] C. Lange, M.W. Barsoum, P. Schaaf, Towards the synthesis of MAX-phase functional coatings by pulsed laser deposition, Appl. Surf. Sci. 254 (2007) 1232–1235. doi:10.1016/j.apsusc.2007.07.156.

[23] E. Pickering, W.J. Lackey, S. Crain, CVD of Ti_3SiC_2, Chem. Vap. Depos. 6 (2000) 289–295. doi:10.1002/1521-3862(200011)6:6<289::AID-CVDE289>3.0.CO;2-4.

[24] M. Sonestedt, J. Frodelius, J.P. Palmquist, H. Högberg, L. Hultman, K. Stiller, Microstructure of high velocity oxy-fuel sprayed Ti_2AlC coatings, J. Mater. Sci. 45 (2010) 2760–2769. doi:10.1007/s10853-010-4263-4.

[25] S. Rech, A. Surpi, S. Vezzù, A. Patelli, A. Trentin, J. Glor, et al., Cold-spray deposition of Ti_2AlC coatings, Vacuum. 94 (2013) 69–73. doi:10.1016/j.vacuum.2013.01.023.

[26] Z.J. Lin, M.S. Li, J.Y. Wang, Y.C. Zhou, Influence of water vapor on the oxidation behavior of Ti_3AlC_2 and Ti_2AlC, Scr. Mater. 58 (2008) 29–32. doi:10.1016/j.scriptamat.2007.09.011.

[27] X.H. Wang, Y.C. Zhou, Oxidation behavior of Ti_3AlC_2 at 1000–1400 °C in air, Corros. Sci. 45 (2003) 891–907. doi:10.1016/S0010-938X(02)00177-4.

[28] D.J. Tallman, B. Anasori, M.W. Barsoum, A Critical Review of the Oxidation of Ti_2AlC, Ti_3AlC_2 and Cr_2AlC in Air, Mater. Res. Lett. 1 (2013) 115–125. doi:10.1080/21663831.2013.806364.

[29] D.J. Tallman, L. He, B.L. Garcia-Diaz, E.N. Hoffman, G. Kohse, R.L. Sindelar, et al., Effect of neutron irradiation on defect evolution in Ti3SiC2 and Ti2AlC, J. Nucl. Mater. 468 (2016) 194–206. doi:http://dx.doi.org/10.1016/j.jnucmat.2015.10.030.

[30] J. Xiao, T. Yang, C. Wang, J. Xue, Y. Wang, Investigations on Radiation Tolerance of Mn+1AXn Phases: Study of Ti_3SiC_2, Ti_3AlC_2,Cr_2AlC, Cr_2GeC, Ti_2AlC, and Ti_2AlN, J. Am. Ceram. Soc. 98 (2015) 1323–1331. doi:10.1111/jace.13450.

[31] H. Högberg, L. Hultman, J. Emmerlich, T. Joelsson, P. Eklund, J.M. Molina-Aldareguia, et al., Growth and characterization of MAX-phase thin films, Surf. Coatings Technol. 193 (2005) 6–10. doi:10.1016/j.surfcoat.2004.08.174.

[32] O. Wilhelmsson, J.-P. Palmquist, E. Lewin, J. Emmerlich, P. Eklund, P.O.Å. Persson, et al., Deposition and characterization of ternary thin films within the Ti–Al–C system by DC magnetron sputtering, J. Cryst. Growth. 291 (2006) 290–300. doi:10.1016/j.jcrysgro.2006.03.008.

[33] W. Garkas, C. Leyens, A. Flores-Renteria, Synthesis and Characterization of Ti_2AlC and Ti_2AlN MAX Phase Coatings Manufactured in an Industrial-Size Coater, Adv. Mater. Res. 89–91 (2010) 208–213. doi:10.4028/www.scientific.net/AMR.89-91.208.

[34] Q.M. Wang, W. Garkas, A.F. Renteria, C. Leyens, H.W. Lee, K.H. Kim, Oxidation behaviour of Ti–Al–C films composed mainly of a Ti2AlC phase, Corros. Sci. 53 (2011) 2948–2955. doi:10.1016/j.corsci.2011.05.033.

[35] Z. Feng, P. Ke, A. Wang, Preparation of Ti_2AlC MAX Phase Coating by DC Magnetron Sputtering Deposition and Vacuum Heat Treatment, J. Mater. Sci. Technol. 31 (2015) 1193–1197. doi:10.1016/j.jmst.2015.10.014.

[36] Z. Feng, P. Ke, Q. Huang, A. Wang, The scaling behavior and mechanism of Ti_2AlC MAX phase coatings in air and pure water vapor, Surf. Coatings Technol. 272 (2015) 380–386. doi:10.1016/j.surfcoat.2015.03.037.

[37] C. Walter, C. Martinez, T. El-Raghy, J.M. Schneider, Towards large area MAX phase coatings on steel, Steel Res. Int. 76 (2005) 225–228. http://cat.inist.fr/?aModele=afficheN&cpsidt=16530247 (accessed March 9, 2015).

[38] Z. Zhang, H. Jin, J. Chai, J. Pan, H.L. Seng, G.T.W. Goh, et al., Temperature-dependent microstructural evolution of Ti_2AlN thin films deposited by reactive magnetron sputtering, Appl. Surf. Sci. 368 (2016) 88–96. doi:10.1016/j.apsusc.2016.01.229.

[39] J. Rosen, P.O.Å. Persson, M. Ionescu, A. Kondyurin, D.R. McKenzie, M.M.M. Bilek, Oxygen incorporation in Ti_2AlC thin films, Appl. Phys. Lett. 92 (2008) 064102/1-064102/3. doi:10.1063/1.2838456.

[40] M.D. Tucker, P.O.Å. Persson, M.C. Guenette, J. Rosén, M.M.M. Bilek, D.R. McKenzie, Substrate orientation effects on the nucleation and growth of the Mn+1AXn phase Ti_2AlC, J. Appl. Phys. 109 (2011) 14903. doi:10.1063/1.3527960.

[41] J. Frodelius, M. Sonestedt, S. Björklund, J.P. Palmquist, K. Stiller, H. Högberg, et al., Ti_2AlC coatings deposited by High Velocity Oxy-Fuel spraying, Surf. Coatings Technol. 202 (2008) 5976–5981. doi:10.1016/j.surfcoat.2008.06.184.

[42] M. Sonestedt, J. Frodelius, M. Sundberg, L. Hultman, K. Stiller, Oxidation of Ti_2AlC bulk and spray deposited coatings, Corros. Sci. 52 (2010) 3955–3961. doi:10.1016/j.corsci.2010.08.004.

[43] M. Hopfeld, R. Grieseler, T. Kups, M. Wilke, P. Schaaf, Thin film synthesis of Ti_3SiC_2 by rapid thermal processing of magnetron-sputtered Ti-C-Si multilayer systems, Adv. Eng. Mater. 15 (2013) 269–275. doi:10.1002/adem.201200180.

[44] J. Robertson, Diamond-like amorphous carbon, Mater. Sci. Eng. R Reports. 37 (2002) 129–281. doi:10.1016/S0927-796X(02)00005-0.

[45] M. Fröhlich, Investigations on the oxidation behavior of MAX-phase based Ti_2AlC coatings on γ-TiAl, in: Ceram. Eng. Sci. Proc., 2010: pp. 161–169. http://www.scopus.com/inward/record.url?eid=2-s2.0-79952404712&partnerID=tZOtx3y1.

[46] A. Ferrari, J. Robertson, Interpretation of Raman spectra of disordered and amorphous carbon, Phys. Rev. B. 61 (2000) 14095–14107. doi:10.1103/PhysRevB.61.14095.

[47] J. Spanier, S. Gupta, M. Amer, M. Barsoum, Vibrational behavior of the Mn+1AXn phases from first-order Raman scattering (M=Ti,V,Cr, A=Si, X=C,N), Phys. Rev. B. 71 (2005) 2–5. doi:10.1103/PhysRevB.71.012103.

[48] V. Vishnyakov, O. Crisan, P. Dobrosz, J.S. Colligon, Ion sputter-deposition and in-air crystallisation of Cr2AlC films, Vacuum. 100 (2014) 61–65. doi:10.1016/j.vacuum.2013.07.045.

[49] H.L. Ma, J.Y. Yang, Y. Dai, Y.B. Zhang, B. Lu, G.H. Ma, Raman study of phase transformation of TiO_2 rutile single crystal irradiated by infrared femtosecond laser, Appl. Surf. Sci. 253 (2007) 7497–7500. doi:10.1016/j.apsusc.2007.03.047.

[50] M. V. Klein, J.A. Holy, W.S. Williams, Raman scattering induced by carbon vacancies in TiCx, Phys. Rev. B. 17 (1978) 1546–1556. doi:10.1103/PhysRevB.17.1546.

[51] V. Presser, M. Naguib, L. Chaput, A. Togo, G. Hug, M.W. Barsoum, First-order Raman scattering of the MAX phases: Ti_2AlN, $Ti_2AlC_{0.5}N_{0.5}$, Ti_2AlC, $(Ti_{0.5}V_{0.5})_2AlC$, V_2AlC, Ti_3AlC_2, and Ti_3GeC_2, J. Raman Spectrosc. 43 (2012) 168–172. doi:10.1002/jrs.3036.

[52] H. Watanabe, N. Yamada, M. Okaji, Linear thermal expansion coefficient of silicon from 293 to 1000 K, Int. J. Thermophys. 25 (2004) 221–236. doi:10.1023/B:IJOT.0000022336.83719.43.

[53] M. Barsoum, I. Salama, T. El-Raghy, J. Golczewski, H. Seifert, F. Aldinger, et al., Thermal and electrical properties of Nb_2AlC, $(Ti, Nb)_2AlC$ and Ti_2AlC, Metall. Mater. Trans. A. 33 (2002) 2775–2779. doi:10.1007/s11661-002-0262-7.

[54] A. Abdulkadhim, M. to Baben, T. Takahashi, V. Schnabel, M. Hans, C. Polzer, et al., Crystallization kinetics

of amorphous Cr_2AlC thin films, Surf. Coatings Technol. 206 (2011) 599–603. doi:10.1016/j.surfcoat.2011.06.003.

[55] Y. Bai, X. He, Y. Li, C. Zhu, S. Zhang, Rapid synthesis of bulk Ti_2AlC by self-propagating high temperature combustion synthesis with a pseudo–hot isostatic pressing process, J. Mater. Res. 24 (2011) 2528–2535. doi:10.1557/jmr.2009.0327.

[56] X. Wang, Y. Zhou, Solid ± liquid reaction synthesis and simultaneous densification of polycrystalline Ti_2AlC, Zeitschrift Für Met. 93 (2002) 2–7.

[57] J. Zhu, J. Gao, J. Yang, F. Wang, K. Niihara, Synthesis and microstructure of layered-ternary Ti_2AlC ceramic by high energy milling and hot pressing, Mater. Sci. Eng. A. 490 (2008) 62–65. doi:10.1016/j.msea.2008.01.017.

[58] V.T. Witusiewicz, B. Hallstedt, A.A. Bondar, U. Hecht, S.V. Sleptsov, T.Y. Velikanova, Thermodynamic description of the Al–C–Ti system, J. Alloys Compd. 623 (2015) 480–496. doi:10.1016/j.jallcom.2014.10.119.

[59] J.P. Palmquist, S. Li, P.O.Å. Persson, J. Emmerlich, O. Wilhelmsson, H. Högberg, et al., Mn+1AXn phases in the Ti-Si-C system studied by thin-film synthesis and ab initio calculations, Phys. Rev. B - Condens. Matter Mater. Phys. 70 (2004) 1–13. doi:10.1103/PhysRevB.70.165401.

[60] T. Joelsson, A. Flink, J. Birch, L. Hultman, Deposition of single-crystal Ti2AlN thin films by reactive magnetron sputtering from a 2Ti:Al compound target, J. Appl. Phys. 102 (2007) 74918. doi:10.1063/1.2785958.

[61] J.P. Palmquist, U. Jansson, T. Seppänen, P.O.Å. Persson, J. Birch, L. Hultman, et al., Magnetron sputtered epitaxial single-phase Ti_3SiC_2 thin films, Appl. Phys. Lett. 81 (2002) 835–837. doi:10.1063/1.1494865.

[62] I. Petrov, P.B. Barna, L. Hultman, J.E. Greene, Microstructural evolution during film growth, J. Vac. Sci. Technol. A Vacuum, Surfaces, Film. 21 (2003) S117. doi:10.1116/1.1601610.

[63] Y. Zhou, Z. Sun, Microstructure and mechanism of damage tolerance for Ti_3SiC_2 bulk ceramics, Mater. Res. Innov. 2 (1999) 360–363. doi:10.1007/s100190050114.

[64] J. Wang, J. Wang, Y. Zhou, Stable $M_2AlC(0001)$ surfaces (M = Ti, V and Cr) by first-principles investigation, J. Phys. Condens. Matter. 20 (2008) 225006. doi:10.1088/0953-8984/20/22/225006.

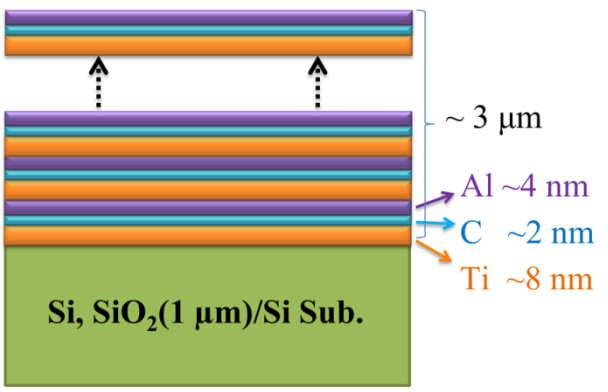
~ 3 µm
Al ~4 nm
C ~2 nm
Ti ~8 nm
Si, SiO2(1 µm)/Si Sub.

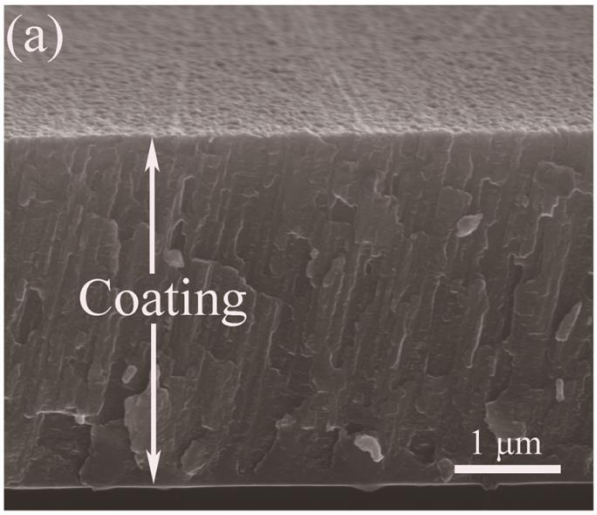
(a)
Coating
1 µm

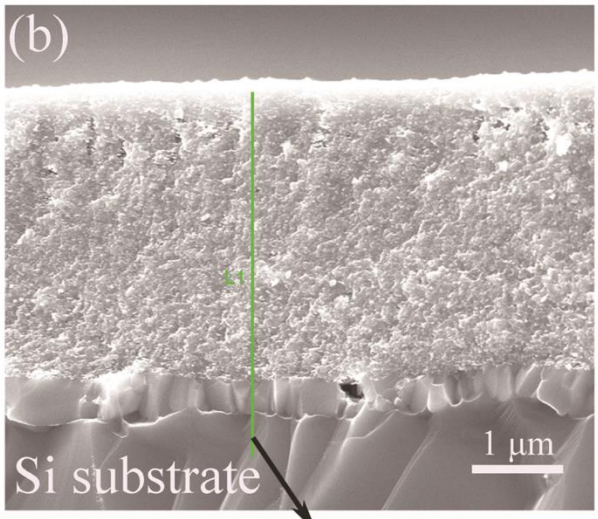
(b)
1 µm
Si substrate

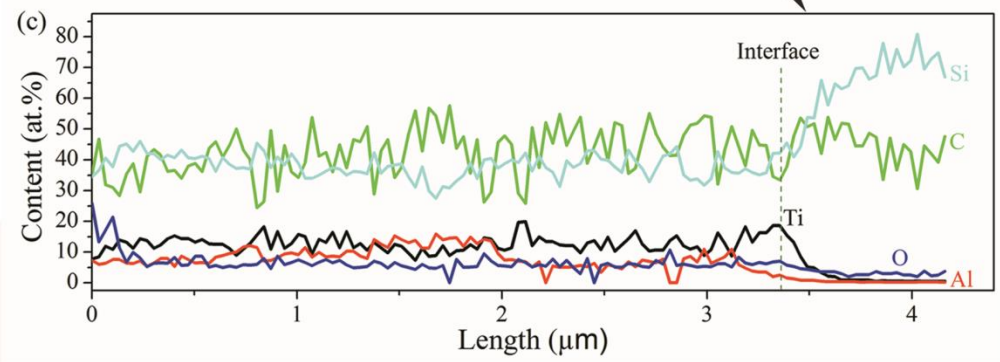
(c)
Content (at.%)
Length (µm)
Interface
Si
C
Ti
O
Al

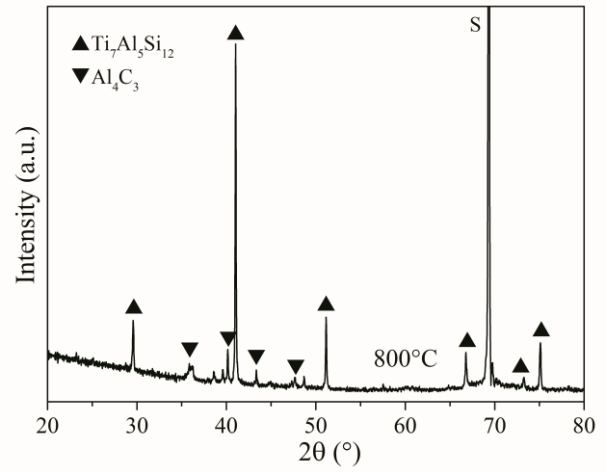
Ti7Al5Si12
Al4C3
S
800°C
Intensity (a.u.)
2θ (°)

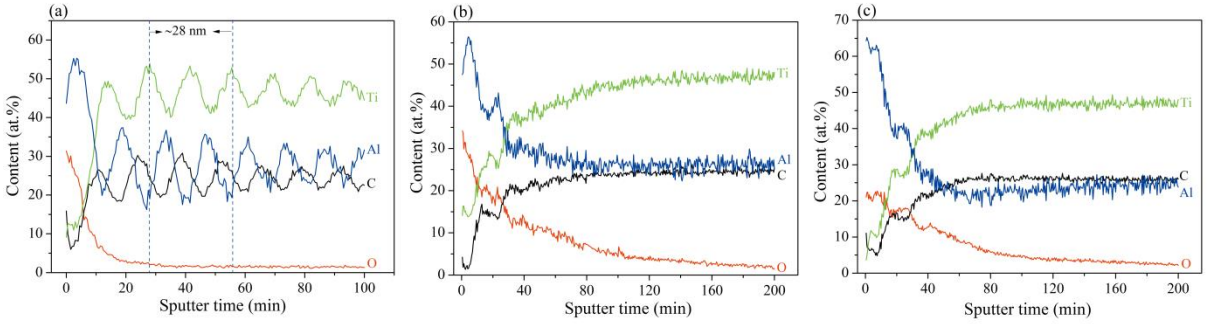
(a)
~28 nm
Ti
Al
C
O
Content (at.%)
Sputter time (min)
(b)
Ti
Al
C
O
Content (at.%)
Sputter time (min)
(c)
Ti
C
Al
O
Content (at.%)
Sputter time (min)

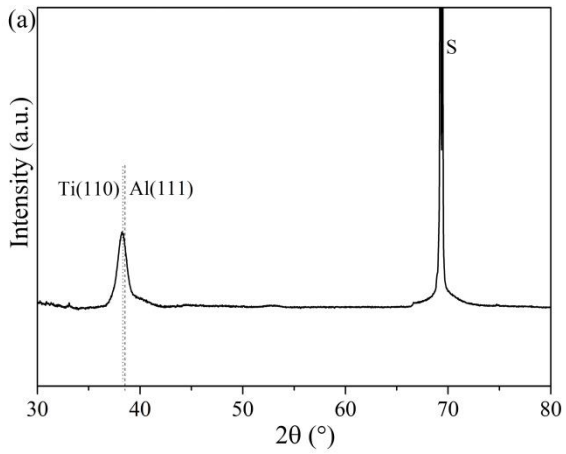
(a)
S
Ti(110)
Al(111)
Intensity (a.u.)
2θ (°)

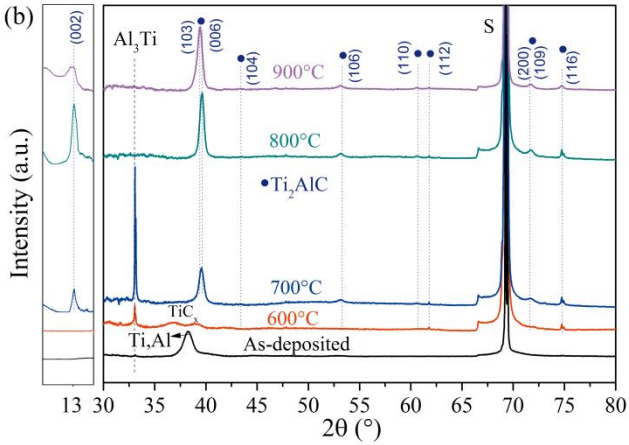
(b)
(002)
Al3Ti
(103)
(006)
(104)
(106)
(110)
(112)
S
(200)
(109)
(116)
900°C
800°C
•Ti2AlC
700°C
TiCx
600°C
Ti3Al
As-deposited
Intensity (a.u.)
2θ (°)

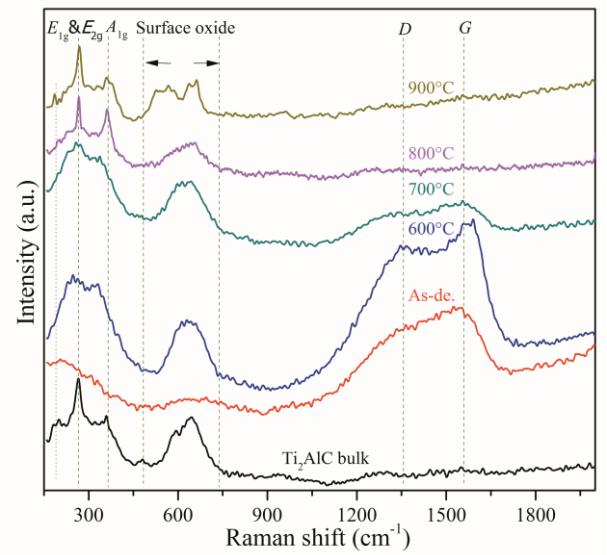
E1g &E2g
A1g
Surface oxide
D
G
900°C
800°C
700°C
600°C
As-de.
Ti2AlC bulk
Intensity (a.u.)
Raman shift (cm-1)

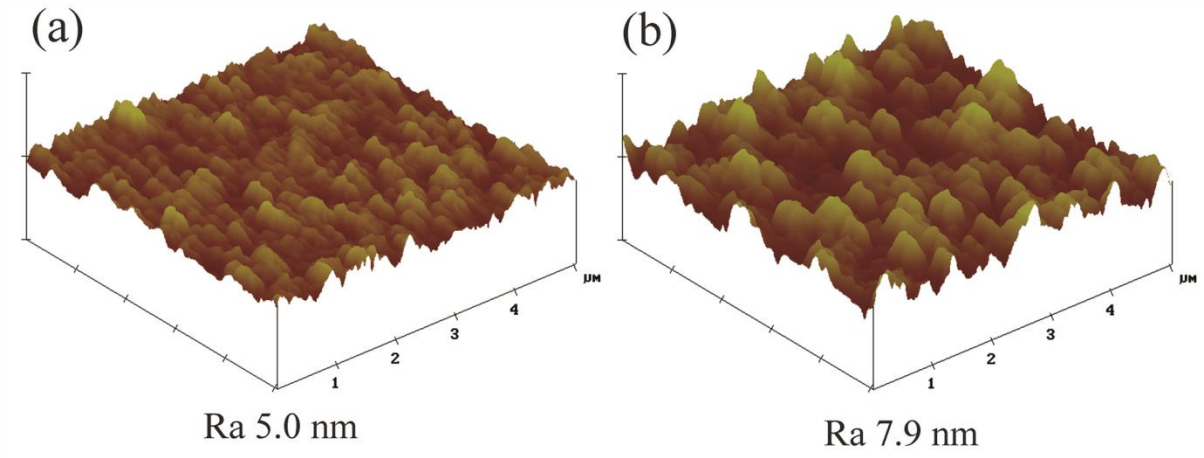
(a)
(b)
μm
Ra 5.0 nm
Ra 7.9 nm

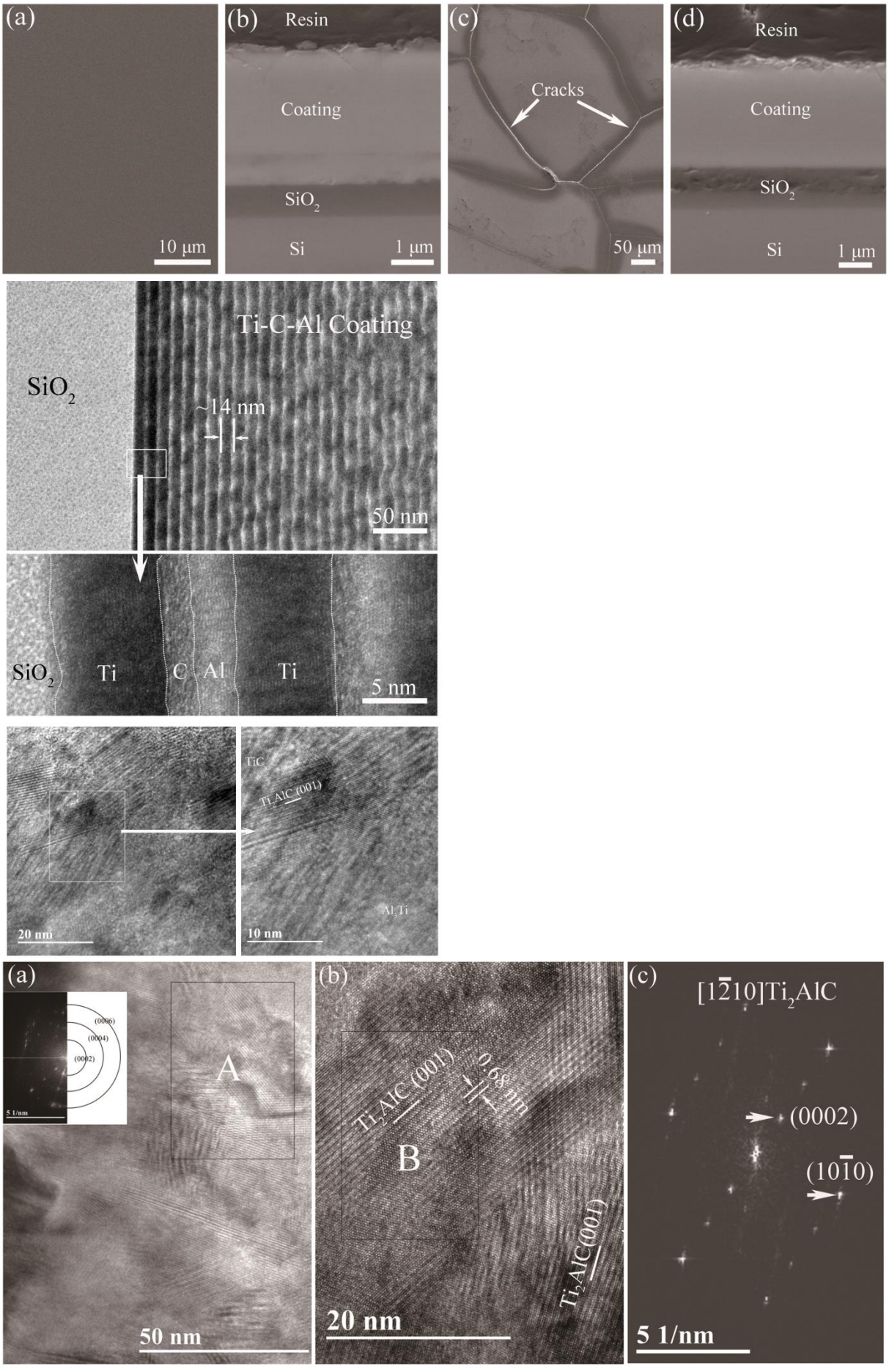
(a)
10 μm
(b)
Resin
Coating
SiO2
Si
1 μm
(c)
Cracks
50 μm
(d)
Resin
Coating
SiO2
Si
1 μm
Ti-C-Al Coating
SiO2
~14 nm
50 nm
SiO2
Ti
C
Al
Ti
5 nm
20 nm
TiC
Ti2AlC (001)
Al Ti
10 nm
(a)
(0006)
(0004)
(0002)
5 1/nm
A
50 nm
(b)
Ti2AlC (001)
0.68 nm
B
Ti2AlC (001)
20 nm
(c)
[1$\bar{2}$10]Ti2AlC
(0002)
(10$\bar{1}$0)
5 1/nm

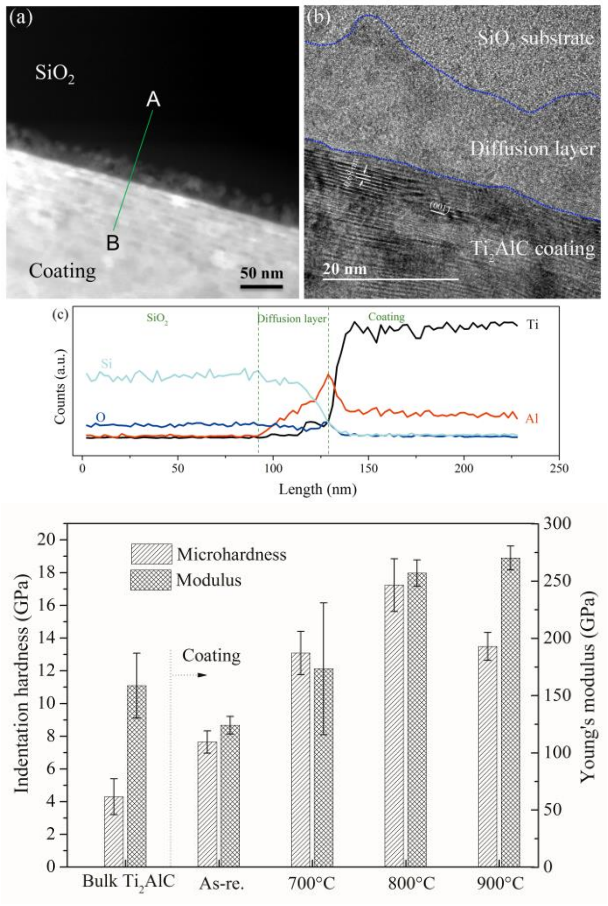

Figure captions

Fig.1 Schematic view of the design of the elemental multilayer system on two different substrates.

Fig.2 SEM cross-sectional images of the coatings on Si and EDS line scan along the cross-section. (a) as-deposited coating, (b) coating annealed at 800°C, (c) EDS line-scan of the 800°C annealed coating along the cross-sectional line in (b) from up to bottom.

Fig.3 XRD pattern of the coating on Si after annealing at 800°C. S for substrate.

Fig.4 AES elemental depth profiles of coatings on SiO_2/Si substrate. (a) as-deposited, (b) annealed at 700°C, (c) annealed at 800°C.

Fig.5 XRD patterns of coating on SiO_2/Si substrate. (a) as-deposited coating, (b) annealed coatings from 600°C to 900°C. Ti_2AlC (●), S for substrate.

Fig.6 Raman spectra for commercial bulk Ti_2AlC ceramic from Kanthal/Sweden, and as-deposited and annealed coatings on SiO_2/Si substrates.

Fig.7 AFM topographical images of coatings on SiO_2/Si substrate. (a) as-deposited, (b) 800°C annealed. The vertical grid is 100 nm.

Fig.8 SEM images of the coating on SiO_2/Si substrate. (a) surface top view and (b) cross section view of as-deposited coating, (c) surface top view and (d) cross section view of 800°C annealed coating.

Fig.9 Bright-field TEM images of as-deposited multilayer Ti-C-Al coating on SiO_2/Si substrate.

Fig.10 Bright-field TEM images of a coating on SiO_2/Si substrate after annealing at 700°C.

Fig.11 TEM images of coating on SiO_2/Si substrate after annealing at 800°C. (a) plan-view of bright-field image with FFT image inserted, (b) HRTEM image of area A in (a), (c) FFT image of area B in (b).

Fig.12 A dark field STEM (HAADF) and HRTEM images of coating-substrate interface after annealing at 800°C. (a) HAADF image, (b) a plan-view bright-field HRTEM image, (c) elemental profiles along the line in (a) from A to B.

Fig.13 Indentation hardness and reduced Young's modulus of bulk Ti_2AlC ceramic and coatings synthesized in this study.